Testing of a background classification algorithm for use with dual-polarized radars in determining precipitation type at the surface

HD Reeves, TJ Schuur, AV Ryzhkov, KL Elmore, J Krause, KL Ortega
NOAA/NSSL and OU/CIMMS

1. Introduction

The NWS is required to provide precipitation type guidance within 200 km of all radars. This is a rather difficult challenge primarily because radars cannot see all the way to the surface and so elevated melting layers may not be detected and because surface observations (ASOS) are rather sparsely spaced. Additionally, ASOS are known to have some biases in detecting freezing rain and are unable to detect ice pellets. A new winter surface classification algorithm is under development at NSSL. This poster presents details important to the development of one phase (the generation of a background class) of this algorithm.

2. Operational Progression

The steps for creating a conus-wide precipitation type analyses are as follows. Step 1: Create a conus-wide background classification (or first-guess) of precipitation type using numerical model analyses or short-range forecasts. Step 2: Port the background classification into the ORPG and use observed radar data to filter out areas where precipitation is not occurring. Step 3: Use dual-polarized observations to refine the background class. Step 4: Export the final classification as a stage II product that can be viewed by forecasters. The stage II product can be "stitched" together to create a conus-wide precipitation-type analysis that is updated in real time and provides forecasters with a storm-wide view of the event as it is evolving.

The aim of this project is to assess limitations that are imposed while creating a background class.

3. The choice of background classification algorithm

There are two approaches to creating a background class. The explicit approach uses model forecasts of hydrometeor mixing ratios as the primary means to distinguish between precipitation type categories. Although this method provides a classification that is consistent with the model-forecast (or analyzed) wind, thermal, and hydrometeor fields if the model fails to produce precipitation in the correct location, then no background class is available. Earlier work demonstrates the background class is necessary. The implicit approach, which is the approach used in this project, uses profiles of wetbulb temperature, humidity, etc to infer the precipitation type at the ground. There are five implicit schemes that are tested here.

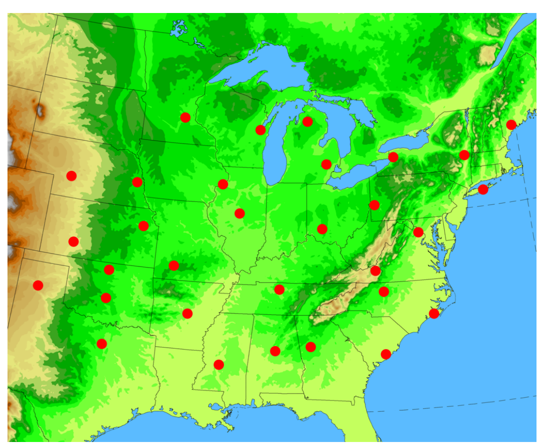

Figure 1: Locations of sounding sites used in the validation of the background algorithms.

These are the Baldwin1, Baldwin2 (B1, B2; Bald-win et al. 1984), Bourgouin (BG; Bourg-ouin 2000), Ramer (RA; Ramer 1993), and NSSL (NS; Schuur et al. 2012) schemes. The B1 and B2 schemes are identical save for the way in which snow (SN) and ice pellets (IP) are discriminated from one another. These schemes diagnose four categories of precipitation: SN, rain (RA), IP, and freezing rain (FZ). The Bg scheme has the same four categories when used operationally. However, it has certain conditions for which IP and FZ cannot be discriminated. In the operational version of the code, one or the other type is randomly selected. For the purposes of this study, the Bg code is revised to produce an IP/FZ mix in such circumstances. The RA and NS schemes diagnose five categories: the same four mentioned above plus a IP/FZ mix.

In order to gauges which algorithm performs best, soundings that occur coincident with observations of IP and FZ are collected over a ten-year period. Any time such a sounding is identified, all sites are examined and any sites where SN or RA occur are also collected. The sites used are shown in Fig. 1. Profiles of wetbulb temperature along with the number of soundings for each sounding class are provided in Fig. 2. Only those sites that have a human observer are able to report IP, leading to fewer IP profiles than for the other classes.

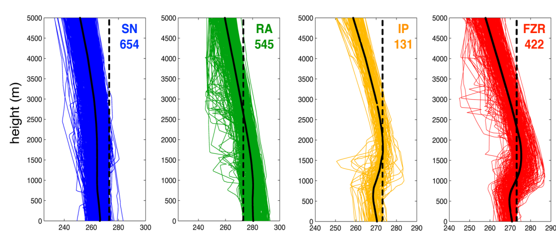

Figure 2: Observed wetbulb temperature profiles for the SN, RA, IP and FZ profiles (colored curves). Means are shown as thick, solid lines. The 273-K isotherm is given as a dashed line.

Also note that the primary distinction between IP and FZ is the depth and maximum temp-erature of the elevated warm layer.

Table 1 shows the hit rates for each algorithm. For all algorithms, the hit rates for SN and RA are quite high. Biases become more evident through consideration of the hit rates for IP and FZ. For example, the B1 scheme has a known bias toward IP, leading to rather high hit rates for this class. This comes at a cost to the scheme's ability to correctly diagnose SN and FZ. The NS scheme also appears to have a rather high bias toward diagnosing the IP/FZ mix, causing it to have lower hit rates for the pure designations of IP and FZ. Most schemes have low hit rates for IP and FZ. Deeper inspection reveals that IP are most commonly misdiagnosed as FZ and vice-versa.

Table 1: The hit rates for the different algorithms. In Bg, NS, and RA, the second value corresponds to the hit rate if one assumes the IP/FZ mix is a hit (if that category is diagnosed).

	SN	RA	IP	FZ
B1	86.7	96.1	89.6	28.4
B2	97.1	96.1	56.0	28.4
Bg	92.6	96.1	50.4/60.0	48.8/55.7
NS	94.1	96.4	26.4/70.4	40.3/78.9
RA	94.9	99.6	25.6	65.4/66.1

As one might expect, the horizontal distribution of precipitation type can vary from scheme to scheme. This is demonstrated using the background class (as calculated using the Rapid-Refresh analysis) at 0300 UTC 22 Feb 2013. At this time, the B1 and B2 schemes have a simple RA-to-SN transition over southern Kentucky (Figs. 3a,b). The Bg scheme has a transition zone that includes IP, IP/FZ mix, and FZ that extends from southern Indiana/Ohio to southern Kentucky (Fig. 3c). The NS scheme has a broader transition zone that is shunted slightly west and extends farther south than that in Bg (Fig. 3d). Last, the RA scheme produces a zone of FZ over western Kentucky and southern Indiana (Fig. 3e).

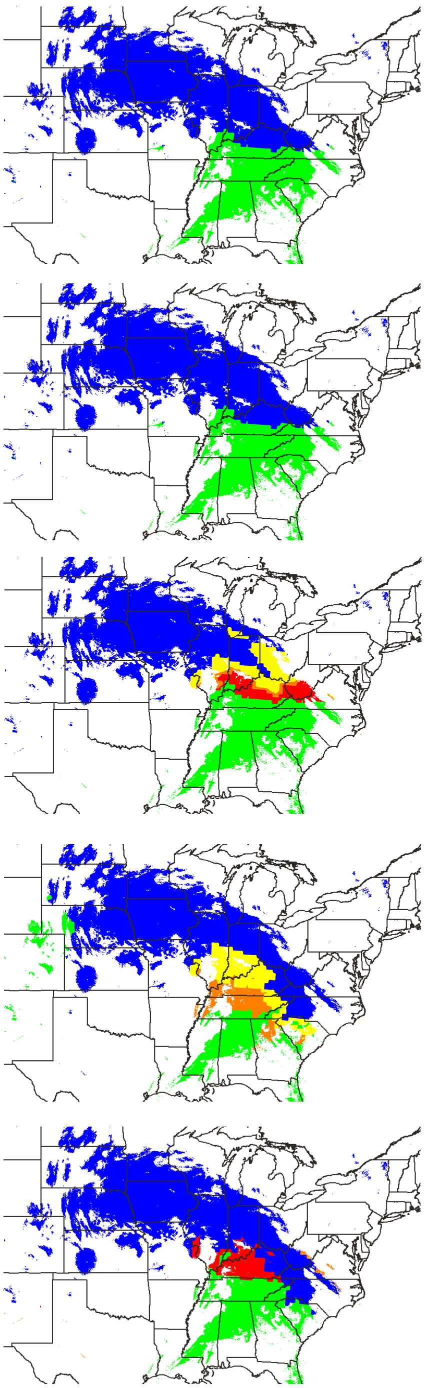

Figure 3: The precipitation type at 0300 UTC 22 Feb 2013 created using the Rapid-Refresh analyses. Blue-SN, green-RA, yellow-IP, red-FZ, orange-IP/FZ mix. The schemes are shown in the following order: B1, B2, Bg, NS, and RA.

The analyses in Fig. 3 can be validated against observations collected as a part of the Precipitation Identification Near the Ground (PING; https://www.nssl.noaa.gov/projects/ping; Elmore et al. 2013) project. The PING project collects crowd-sourced observations of precipitation type that are reported by citizen observers. The PING observations of precipitation type between 0200 and 0400 UTC 22 Feb are provided in Fig. 4 At this time, there is a broad transition zone of various forms of intermediate precipitation types (IP, FZ, IP/SN mix, etc) over central Illinois, Indiana, southern Ohio, and northeastern Kentucky. It appears, then, that none of the algorithms were entirely accurate in their placement of the transition zone. However, the NS scheme is the closest and, by virtue of its rather broad region of IP/FZ mix, best captures the character of the observed precipitation type. Similar comparisons of other events yields the same result.

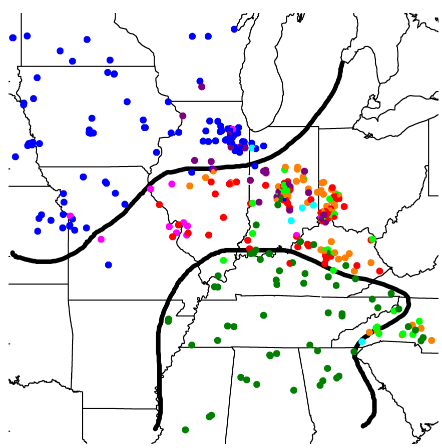

Figure 4: PING observations of precipitation type between 0200 and 0400 UTC 22 Feb 2013. The colors are as in Fig. 3.

4. Horizontal variability in precipitation type

The high spatial variability of precipitation type in the transition zone of Fig. 4 is a curiosity and prompts one to question what the horizontal variability in precipitation type is like. To better gauge this, observations within prescribed radii of each PING observation of SN, RA, IP, and FZ are collected. The percentage of these that agree with the given observation are calcul-calculated and presented in graphical form in Fig. 5. For all categories, the rate of agreement decreases as the distance (or radii) increases. The SN and RA observations have a comparatively low horizontal variability as demonstrated by the higher rates of agreement while IP and FZ have rather high variability.

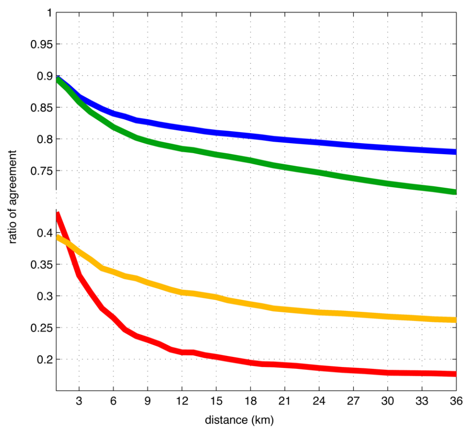

Figure 5: Voroni analysis of the spatial variability of PING observations as a function of the radius away from an observation of a given class.

The exact rates of agreement for certain distances are provided in Table 2. For a radius of 3 km (the grid spacing of the high-resolution Rapid-Refresh model), the rate of agree-ment for FZ is only 33%. In other words, for every FZ observation, only one-third of the area within 3 km of that observation is also getting FZ. As the radius is increased to 5 km (the average downwind drift of a radiosonde in the lowest half of the troposphere), the agreement for FZ drops to 28%. For a distance of 13 km (the grid spacing of the Rapid-Refresh model), the agreement drops to 21%.

The above may indicate one may never see hit rates for FZ and IP that rival those for SN and RA, no matter what approach is taken for the background classification algorithm. A detailed examination of the forms of precipitation that occur in close proximity to FZ and IP suggest that these types of precipitation usually occur as a part of a mix that is dominated by FZ and IP and to a lesser extend, SN and RA. Hence, the choice to diagnose an IP/FZ mix may pro-vide the public with the most accurate description of the current weather conditions.

Table 2: The rates of agreement for observations within a given radii of SN, RA, FZ, and IP observations.

	3 km	5 km	13 km
SN	87%	85%	81%
RA	86%	83%	78%
IP	37%	34%	30%
FZ	33%	28%	21%

There are two caveats to consider from the above arguments. The first is that the PING observations are heavily weighted toward urban areas (not shown). One would expect a higher spatial variability in urban areas given the variations in building density, tree maturity, traffic, etc. It is unknown to what degree the precipitation type varies in rural areas. Second, the PING program has only been in existence nationwide for one winter season. There were no broad scale IP or FZ events during this season.

5. Analysis/forecast uncertainty

To gauge the effects of the analysis and forecast uncertainty on the accuracy of a given algorithm, the Rapid-Update-Cycle (RUC; Benjamin 1989) model analyses and 01-, 06-, and 12-h forecast soundings that correspond to the observed soundings in Fig. 2 are collected. The wetbulb profiles for these soundings are provided in Fig. 6. Notice that the distributions and means are very similar to the observed soundings. Yet, there are subtle variations between an observed sounding and its RUC counterparts. This is exhibited using the unbiased kernel density distributions of the difference between the RUC analyses/forecasts and the observations in Fig. 7. Only the distributions at the surface are shown, but similar distributions are found throughout the lowest 5000 m above ground level. Note that the maximum density decreases and the spread increases as lead time increases. This is consistent with initial condition uncertainty and error growth in mesoscale models.

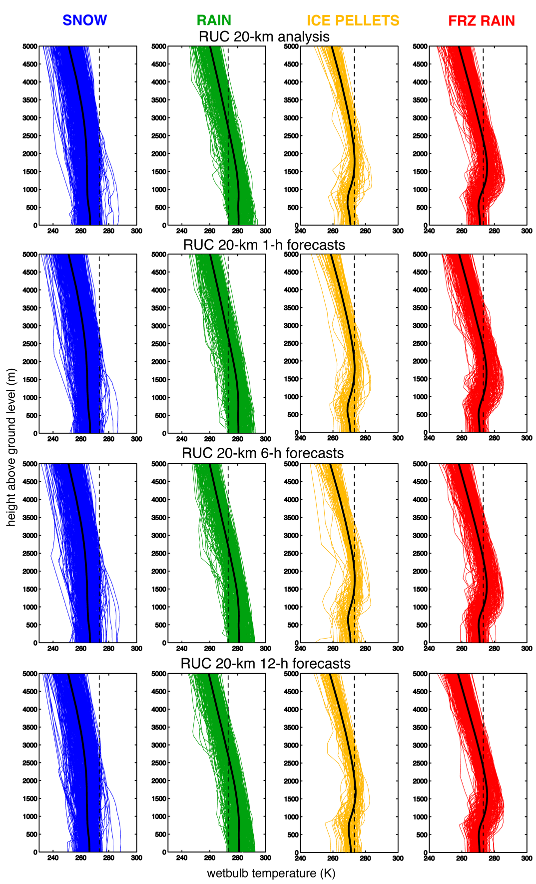

Figure 6: Wetbulb temperature profiles from the RUC model analyses and forecasts with select lead times (colored lines). Means are given as thick black curves and the 273-K isotherm by the dashed line.

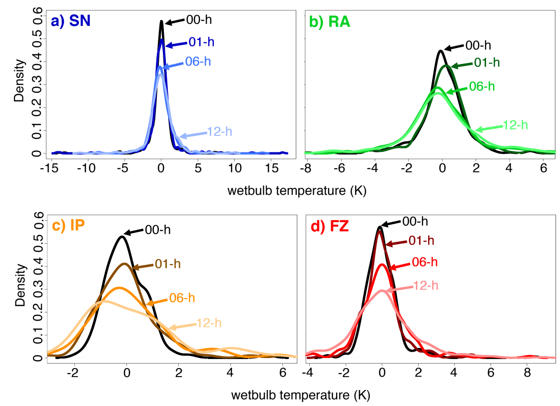

Figure 7: Kernel density distributions for the different precipitation types and forecast lead times.

The unbiased kernel density distributions are used to create an array of perturbations on the observed soundings. Allowing each sounding to have 1000 perturbations. These sounding arrays represent the range of likely analyses and forecasts that could be expected for this modeling system and others with similar grid spacings and physical parameterizations. The arrays of soundings are then fed to each of the background algorithms described in Section 3 and hit rates calculated. The hit rates are provided in Table 3. DISCUSS

Table 3: The hit rates for the different algorithms using the perturbed soundings. In Bg, NS, and RA, the second value corresponds to the hit rate if one assumes the IP/FZ mix is a hit (if that category is diagnosed).

	SN	RA	IP	FZ
B1	66.3	89.7	3.9	20.4
B2	63.8	94.8	60.8	27.5
Bg	87.9	97.8	48.9/60.0	41.5/47.1
NS	89.8	96.8	18.2/50.8	24.5/54.3
RA	97.4	93.0	6.6/20.0	23.0/42.3

6. Conclusions

Various contributors to decreased accuracy in a background classification algorithm for the new winter surface hydrometeor classification algorithm have been considered.

These include the uncertainty introduced by the choice of algorithm, the horizontal variability of the precipitation type, and the analysis/forecast uncertainty. All things combined, it is clear that SN and RA are able to well detected regardless of the above uncertainties. However, IP and FZ suffer substantially. Using a mixed category helps improve hit rates in a statistical sense, but it is still desirable to have an independent FZ category as pure FZ storms can be catastrophic. More attention will be paid to broad scale FZ events in the future to see how these can be effectively treated.

References

Baldwin, M., R. Treadon, and S. Contorno, 1994: Precipitation type prediction using a decision tree approach with NMCs mesoscale eta model. Preprints. *10th Conf. on Numerical Weather Prediction*, Portland, OR, Amer. Meteor. Soc., 30-31.

Benjamin, S.G., 1989: An isentropic mesoα-scale analysis system and its sensitivity to aircraft and surface observations. *Mon. Wea. Rev.,* **117**, 1586-1603.

Bourgouin, P., 2000: A method to determine precipitation type. *Wea. Forecasting*, **15**, 583-592.

Ramer, J., 1993: An empirical technique for diagnosing precipitation type from model output. Preprints. *5th Int. Conf. on Aviation Weather Systems*, Vienna, VA, Amer. Meteor. Soc. 227-230.

Schuur, T.J., H.S. Park, A.V. Ryzhkov, and H.D. Reeves, 2012: Classification of precipitation types during transitional winter weather using the RUC model and polarimetric radar retrievals. *J. Appl. Meteor. Climatology*, **51**, 763-779.